Sedimentary Geology 289 (2013) 194–209

Contents lists available at SciVerse ScienceDirect

Sedimentary Geology

journal homepage: www.elsevier.com/locate/sedgeo

Reworked pyroclastic beds in the early Miocene of Patagonia: Reaction in response to high sediment supply during explosive volcanic events

José I. Cuitiño *, Roberto A. Scasso

Departamento de Ciencias Geológicas, Facultad de Ciencias Exactas y Naturales, Universidad de Buenos Aires, Ciudad Universitaria, Pabellón II, primer piso, Intendente Guiraldes 2160 (C1428EHA), Ciudad Autónoma de Buenos Aires, Argentina
Instituto de Geociencias Básicas, Aplicadas y Ambientales de Buenos Aires (IGeBA), Consejo Nacional de Investigaciones Científicas y Técnicas (CONICET), Argentina

ARTICLE INFO

Article history:
Received 31 May 2012
Received in revised form 25 February 2013
Accepted 3 March 2013
Available online 13 March 2013

Editor: J. Knight

Keywords:
Pyroclastic deposits
Explosive volcanism
Hyperpycnal flows
Fluvial deposits
Patagonia

ABSTRACT

Two meter-scale pyroclastic levels are interbedded within the early Miocene succession of the Estancia 25 de Mayo (*Patagoniense transgression*) and Santa Cruz formations in the foreland Austral (or Magallanes) Basin, Argentina. The Lower Pyroclastic Level (LPL) is a tabular body interbedded within offshore marine deposits, laterally continuous for 30 km and varying in thickness from few centimeters to around 4 m. Grain-size grades from coarse to extremely fine ash with upward-fining along with a northeastern-fining trends. Structureless fine to very fine tuffs dominate and rare parallel laminations are the only tractive sedimentary structures. The Upper Pyroclastic Level (UPL) lies within low energy fluvial deposits and is laterally discontinuous, and it is composed by lenticular bodies reaching a maximum of 15 m thick and 100 m wide, with a concave-up base and a plane top. Grain-size range is similar to the LPL but it coarsens upward. The lower portion of the UPL shows parallel lamination, current ripple lamination and mud drapes with large pumice lapilli and plant debris, whereas the upper portion shows parallel lamination and trough cross-stratification. Both pyroclastic levels are composed mainly of pumice grains and glass shards with minor proportions of quartz and plagioclase crystals and lithic fragments. The LPL shows no mixing with epiclastic material whereas the UPL shows an upward increase in epiclastic material, and an upward increment in the scale of cross-bedding.

The large thickness in relation to the possible emission center and the content of plant debris of the LPL does not suggest a direct, submarine, ash-fallout origin. The LPL is interpreted as a deposit of hyperpycnal-flows generated at the coastal zone when tephra-laden rivers plunged into the ocean. Large amounts of well preserved plant debris support the hypothesis of a terrestrial source of the sediments. The UPL is entirely composed of tractive deposits, so an ash fallout origin is disregarded. This, together with the lenticular shape and the alluvial plain origin of the encasing sediments, suggests accumulation within fluvial channels. Cycles of upper-flow-regime parallel lamination, current-ripple lamination and mud drapes at the lower portion, suggest short-lived turbulent flows that initially filled semi-abandoned channels. They were followed by sheet floods and channel reactivation, expressed by large-scale cross-bedding. The low degree of particle mixing observed in both levels is explained by the inability of streams to erode the substrate as they are suddenly over-saturated with pyroclastic sediments during and after the eruption. The grain-size distribution of the LPL and geochemical data indicate a contemporaneous volcanic source located to the west/southwest in the Andean ranges, where the South Patagonian Batholith is presently located.

1. Introduction

Volcanically-influenced sedimentary settings are complex systems which reflect the addition of volcanic ejecta, succeeding transport and deposition in a wide range of environments, from top of mountain chains to the bathyal ocean (Fisher and Smith, 1991; McPhie et al., 1993; Manville et al., 2009). A unique feature of these systems is that sediment supply is not limited by rates of weathering, erosion, or production of biogenic material, but can be introduced instantaneously and in enormous volumes by volcanic eruptions, overwhelming pre-existing transport systems (Fisher and Smith, 1991; Newhall and Punongbayan, 1996; Manville et al., 2005, 2009).

The stratigraphic record of volcanic regions comprises both syn- and post-eruptive volcaniclastic deposits that result from the immediate or subsequent reworking of this material by surface processes (Smith, 1991; Orton, 1996; Manville et al., 2009). These deposits, accumulated in various and markedly different sedimentary environments, leave a complex stratigraphic and sedimentologic record that

* Corresponding author at: Departamento de Ciencias Geológicas, Facultad de Ciencias Exactas y Naturales, Universidad de Buenos Aires, Ciudad Universitaria, Pabellón II, primer piso, Intendente Guiraldes 2160 (C1428EHA), Ciudad Autónoma de Buenos Aires, Argentina. Tel.: +54 11 1562854266.
E-mail address: joseignacio@gl.fcen.uba.ar (J.I. Cuitiño).

0037-0738/$ – see front matter © 2013 Elsevier B.V. All rights reserved.
http://dx.doi.org/10.1016/j.sedgeo.2013.03.004

varies from proximal coarse volcanic facies (e.g., Smith, 1991) to distal fine-grained volcanic facies (Kataoka, 2005; Kataoka et al., 2009), recording the processes that acted at high altitude subaerial settings (cf., Fisher and Smith, 1991; Smith, 1991) as well as in shallow and deep marine settings (Sigurdsson et al., 1980; Wright and Mutti, 1981; Carey, 2000).

Smith (1991) subdivided volcaniclastic sequences into: i) syn-eruptive units, formed coevally with volcanic activity through the immediate reworking of pyroclastic material, and extending through the period where the landscape is still responding to the hydrological and sedimentary-yield consequences of the eruption; and ii) inter-eruptive sequences, where normal background sedimentary processes occur without a direct volcanic influence.

Most models of syn- or inter-eruptive terrestrial deposits deal with coarse grained material proximal to the volcanic source, reworked by fluvial processes and debris flows (Kuenzi et al., 1979; Smith, 1988, 1991; McPhie et al., 1993; Newhall and Punongbayan, 1996; Zernack et al., 2011). On the contrary, less is known about distal sand-to-mud sized pyroclastic material interacting with fluvial and marine processes (Kataoka, 2005; Manville et al., 2005, 2009; Kataoka et al., 2009).

Meter-thick-scale submarine pyroclast-rich deposits were mostly interpreted as the result of submarine or delta slope failures, or related to submarine or subaerial pyroclastic flows (Sigurdsson et al., 1980; Wright and Mutti, 1981; McPhie et al., 1993). However, during subaerial explosive eruptions a large amount of sediment is supplied by ash fallout to the drainage basins which finally is carried to the ocean resulting in underflows or quasi-steady hyperpycnal flows (Mulder and Syvitski, 1995).

The Cenozoic stratigraphic record of extra-Andean Patagonia is characterized by large amounts of pyroclastic material preserved within many sedimentary units. Particularly, the lower Miocene marine deposits known as the "*Patagoniense transgression*", widely distributed over eastern Patagonia (Fig. 1), present numerous intercalated fine-grained pyroclastic beds and variable proportions of pyroclastic material mixed within other epiclastic sediments (Di Paola and Marchese, 1973; Riggi, 1978; Bellosi, 1995; Crawford et al., 2008). Little is known about their age, source and modes of deposition and preservation, and most of them were interpreted as pyroclastic ash fallout deposits (Di Paola and Marchese, 1973; Riggi, 1978; Crawford et al., 2008). This paper present a detailed facies analysis of two early Miocene thick, distal fine-grained pyroclastic deposits preserved within offshore marine and low energy fluvial environments, and accounts for the processes of reworking, deposition, and preservation that fluvial channel, shorelines and offshore settings imprint on the volcanic-sourced particles, as well as how each sedimentary system reacts against the supply of pyroclastic particles.

2. Geologic framework

The pyroclastic beds studied here are part of the Burdigalian infill of the Austral (or Magallanes) Basin (Cuitiño et al., 2012). This basin is located in the southern portion of the South American Plate, and limited by its west side by the Patagonian–Fueguian Andes (Fig. 2A). This rift-sag to foreland basin contains deep-marine to continental sedimentary units of early Cretaceous to middle Miocene age (Biddle et al., 1986; Arbe, 2002). During the Miocene the succession was thrusted and inverted due to Andean tectonics (Fosdick et al., 2011). In the study area, between Lago Argentino to the north and Sierra Baguales to the south, only the late Cretaceous to Miocene foreland deposits are present (Fig. 2), covered in part by a thick pile of late Cenozoic volcanic lava flows and modern glaciogenic deposits. The pyroclast-rich succession studied herein is composed of the shallow marine Estancia 25 de Mayo Formation (Cuitiño and Scasso, 2010; formerly called the Centinela Formation of Furque and Camacho, 1972), transitionally overlain by the continental Santa Cruz Formation (Fig. 2B; Table 1). The Oligocene fluvial sediments

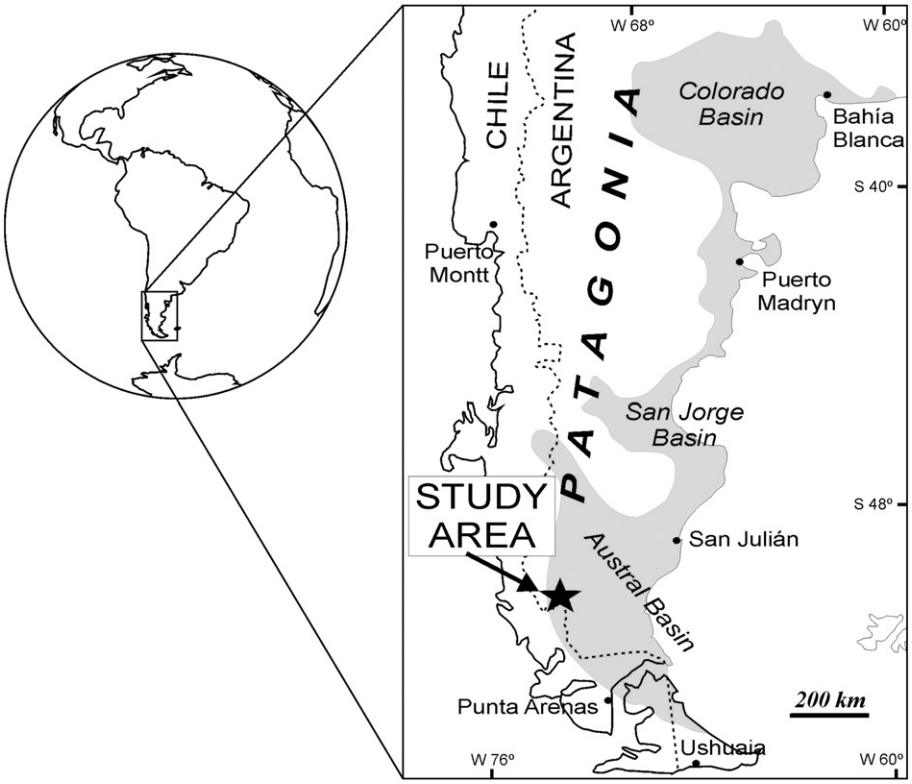

Fig. 1. Location of the study area. The gray area in eastern Patagonia corresponds to the surface inundated by the early Miocene "Patagoniense" transgression. After Malumián et al. (1999).

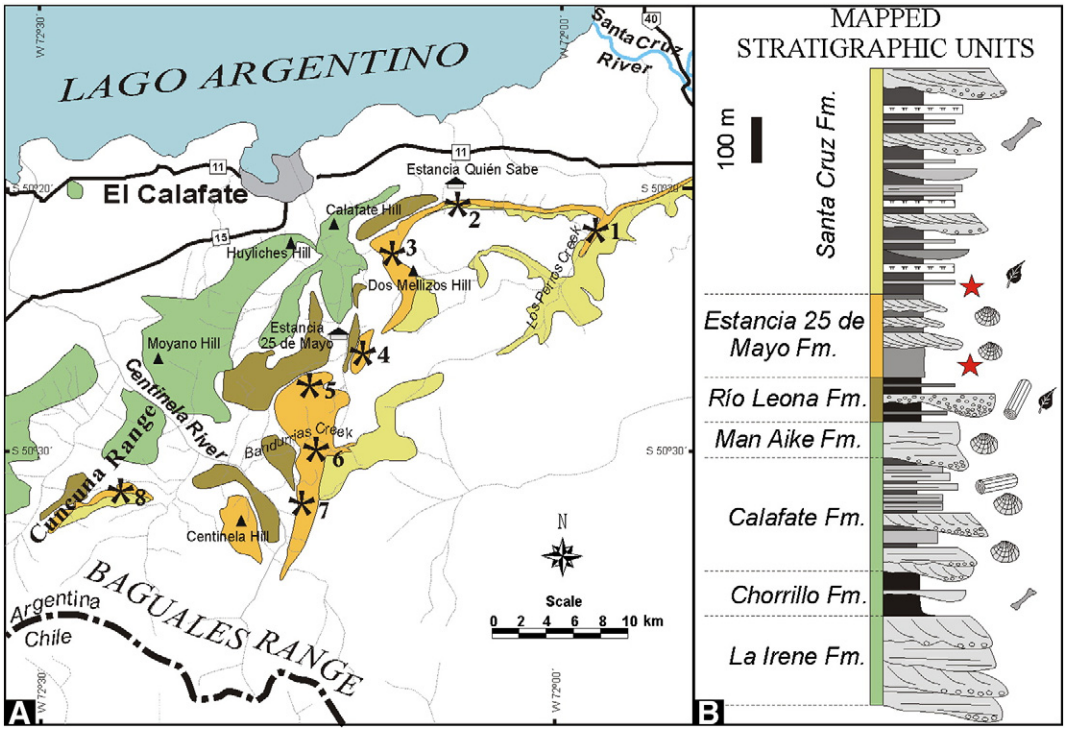

Fig. 2. A) Geologic map of the study area showing the upper Cretaceous to Eocene units (green), the Oligocene Río Leona Formation (brownish), the early Miocene Estancia 25 de Mayo (orange) and Santa Cruz (pale yellow) formations. Numbers (*) indicate positions of the analyzed stratigraphic sections. B) Schematic stratigraphic column of the units mapped in A. Red stars indicate the position of the pyroclastic levels.
Thicknesses and general sedimentary features are compiled from Furque (1973), Macellari et al. (1989), Marenssi et al. (2004, 2005), Casadío et al. (2009), Cuitiño and Scasso (2010), Cuitiño et al. (2012), and this study.

of the Río Leona Formation (Marenssi et al., 2005; Barreda et al., 2009) underlie the Estancia 25 de Mayo Formation (Fig. 2B).

The Estancia 25 de Mayo Formation is part of a local stage known as the "*Patagoniense transgression*", a large Cenozoic marine invasion extensively recorded along the eastern part of Patagonia (Feruglio, 1949; Malumián et al., 1999; Cuitiño et al., 2012). In the southern part of Patagonia the sea reached up to the foothills of the Andes (Malumián et al., 1999; Cuitiño, 2011). One of the distinctive characteristics of these extensive marine beds is the large amount of pyroclastic material preserved either as "pure" (more than 90% of pyroclastic particles) ash layers or mixed with epiclastic sediments (Di Paola and Marchese, 1973; Riggi, 1978; Bellosi, 1995; Malumián et al., 1999; Crawford et al., 2008). The Estancia 25 de Mayo Formation comprises shallow marine to coastal sandstones and mudstones. It was subdivided into two members by Cuitiño and Scasso (2010): the lower Quién Sabe Member and the upper Bandurrias Member (Table 1). The Quién Sabe Member consists of profusely bioturbated, massive, brownish, fine-grained sandstones and siltstones, containing abundant bivalves, gastropods, echinoids and crustaceans (Fig. 3). It was deposited in a low- to moderate-energy, offshore marine environment (Cuitiño and Scasso, 2010; Cuitiño, 2011). The upper Bandurrias Member consists of medium- to coarse-grained sandstones with numerous erosive surfaces, abundant tractive sedimentary structures and moderate to rare bioturbation. It was accumulated in tide-dominated shallow marine to estuarine environments (Cuitiño, 2011). The Santa Cruz Formation is composed of small, channelized sandstone fluvial bodies encased in muddy to fine-grained sandy floodplains with soil development and terrestrial mammal remains (Fig. 3).

The sedimentary package formed by the Estancia 25 de Mayo and Santa Cruz Formations represents a regional progradation event coeval with the tectonic uplift of the Andean Ranges during the early Miocene (Fosdick et al., 2011; Cuitiño et al., 2012), recorded in an orogenic front at least 600 km long running from the north-western region of the Santa Cruz province (and the Aysen region of Chile) to the region of the Magellan's Strait in Chile. Volcanic activity is recorded as intercalated pyroclastic deposits such as those described herein, and plutonic intrusions cropping out to the west along the axis of the South Patagonian Batholith (Hervé et al., 2007).

Table 1
Lithostratigraphic units and their basic lithology and paleoenvironment interpretation.
After Furque, 1973; Marenssi et al., 2005 and Cuitiño and Scasso, 2010.

Age	Lithostratigraphic unit		Lithology	Paleoenvironment
Early Miocene	Santa Cruz Formation		Interbedded sandstones, tuffaceous sandstones and mudstones. Numerous pyroclastic intercalations.	Low-energy fluvial
Early Miocene	Estancia 25 de Mayo Formation	Bandurrias Member	Interbedded cross-bedded sandstones and mudstones. Numerous shell beds.	Nearshore marine, tide dominated.
		Quien Sabe Member	Dominantly mudstones with fine sandstones intercalations. Shell beds.	Offshore to nearshore marine
Late Oligocene	Rio Leona Formation		Interbedded fine conglomerates, sandstones and carbonaceous mudstones.	Low-energy fluvial

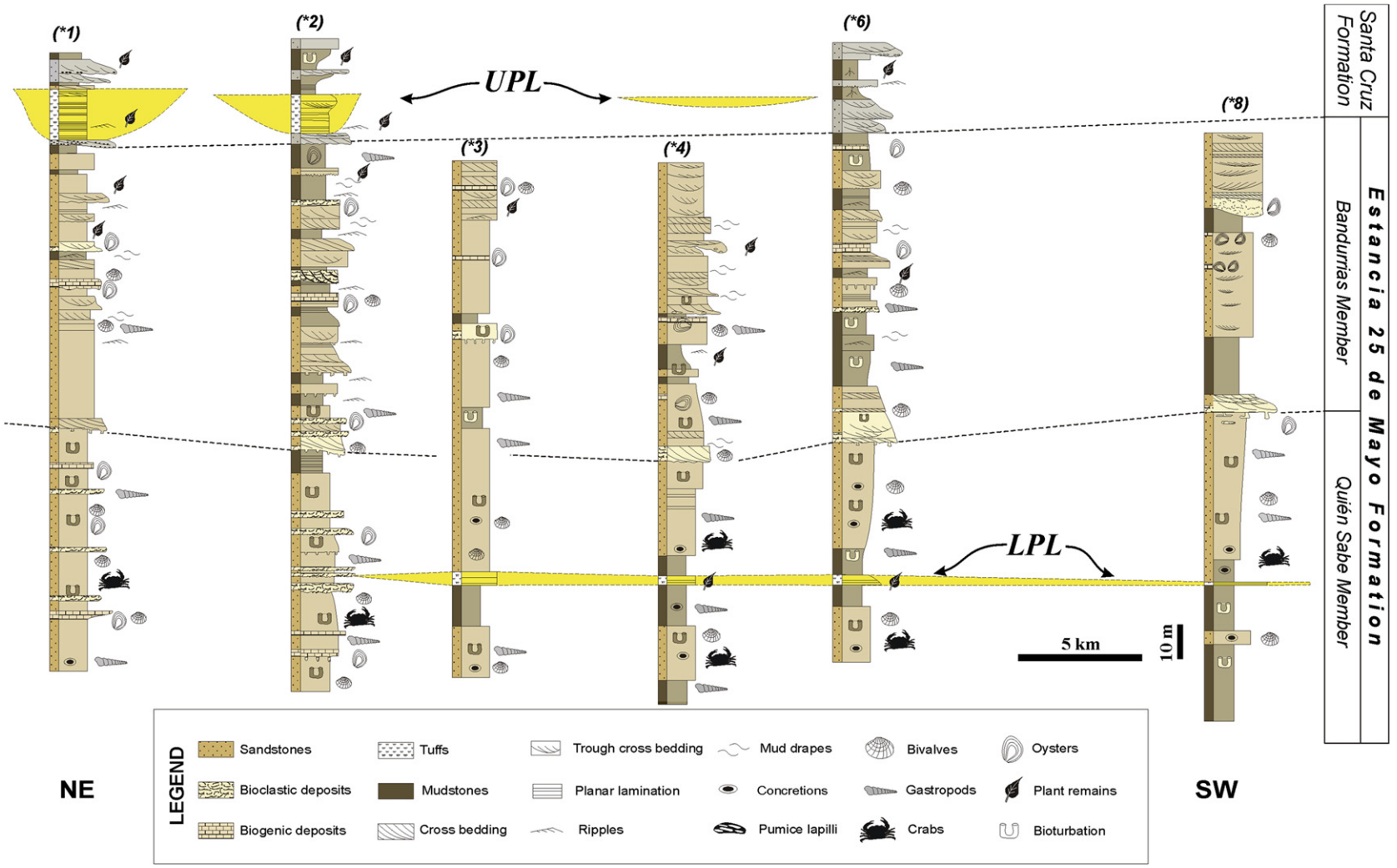

Fig. 3. Cross section showing the main characteristics of the Estancia 25 de Mayo and the base of Santa Cruz formations. Both pyroclastic levels are highlighted in yellow. Numbers above each log indicate the locality as shown in Fig. 1B. For simplicity, logs from localities *5 and *7 are not included in the figure.

3. Methodology

Eight stratigraphic sections (Figs. 2, 3) were measured in good exposures of the pyroclastic deposits, with the scope of determining the palaeoenvironment and sedimentary processes (Figs. 3–5). Hand samples were sliced and polished in order to highlight small-scale sedimentary features and thin sections were used to analyze the fine-scale laminations, grain size, sorting and particle composition within the pyroclastic beds. Volume percent of the rock components were measured by point counting on several thin sections. Organic matter in the Upper Pyroclastic Level and adjacent mudstone beds was analyzed in order to determine the thermal alteration state by means of Vitrinite Reflectance and Thermal Alteration Index (TAI). Macroscopic coal fragments from the UPL were handpicked, mounted on epoxy resin, polished and observed with incident blue-UV light and incident white light. Vitrinite reflectance was measured under standard conditions with a Jena Alumar microscope. Mudstone samples were reacted with HCl/HF and the concentrated kerogen mounted on a palynological preparation for it observation under transmitted light and TAI determination.

Bulk-rock chemical analyses were performed using standard techniques of UV–visible spectroscopy (Si, Al, Ti, Mn, Fe and P), atomic absorption spectrometry (Ca, Mg Na and K), drying at 1000 °C (H_2O^+), drying at 105 °C (H_2O^-) and titration with HCl (CO_2) at the Laboratorio de Análisis de Rocas, Buenos Aires University.

The two studied pyroclastic beds are called here the Lower Pyroclastic Level (LPL) and the Upper Pyroclastic Level (UPL). The term "pyroclastic" is used here for deposits containing a large proportion of particles originated as the result of fragmentation during explosive volcanic eruptions, independent of the mode of transport and final deposition (Fisher and Schmincke, 1984). The term "tuffaceous sandstones" is used for mixed pyroclastic–epiclastic sedimentary rocks. The grain size classification of the pyroclastic deposits is given following White and Houghton (2006) as this classification provides good resolution for sand-sized (and finer) pyroclastic particles.

4. Pyroclastic beds

4.1. Distribution, geometry, and sedimentary features

The two meter-scale pyroclastic beds are vertically separated by 150 m. The pyroclastic beds can be recognized by their pale-yellow to whitish color, contrasting notably with the brownish color of the surrounding sandstones and mudstones. The contacts of the pyroclastic levels with the bedrocks, especially the bases, are sharp and easy to recognize. The LPL is interbedded in the basal section of the Quién Sabe Member and the UPL in the basal section of the Santa Cruz Formation (Fig. 3). The ages of both the LPL and the UPL were determined by means of U–Pb, laser ablation-inductively coupled plasma-mass spectrometry on single zircon grains and the results indicate an age of 19.1 Ma for the LPL and 18.8 Ma for the UPL (Cuitiño et al., 2012). Sr^{87}/Sr^{86} datings from 20 to 18.9 Ma on oyster shells from the marine beds of the Estancia 25 de Mayo Formation agree well with the U–Pb ages (Cuitiño et al., 2012) and confirm the Burdigalian (early Miocene) age for these beds.

4.1.1. Lower Pyroclastic Level

The Lower Pyroclastic Level (LPL) is a tabular bed with subtle thickness variations (Fig. 6A), and it is laterally traceable for more than 30 km in northeast–southwest direction (Figs. 3, 4). It pinches out to the northeast of Dos Mellizos Hill, and at Estancia Quién Sabe the level is stratigraphically equivalent to a monotonous succession of massive, highly bioturbated, fossiliferous, fine-grained tuffaceous sandstones, with many erosional surfaces (Fig. 3). To the southwest it is assumed to continue beyond the Cuncuna Range below modern sedimentary cover deposits.

The LPL lies 30 m above the contact between the Río Leona and Estancia 25 de Mayo Formations, intercalated within muddy to fine-sandy, marine fossiliferous sediments (Figs. 3, 4). Its base is sharp and planar, without any recognizable relief (Figs. 4, 6A–C), and its top gradually mixes with the overlying fine-grained epiclastic sediments (Fig. 4). Its thickness ranges from 0.3 m to the southwest (Cuncuna Range) to nearly 4 m to the northeast (Dos Mellizos Hill; Fig. 4), where it quickly wedges out and disappears. At Estancia Quién Sabe and Los Perros Creek, only diffuse coarse-grained tuffaceous layers are present.

This level shows two general grain-size trends: 1) a vertical, fining-upward (normal grading) trend, in which coarse to very coarse tuffs in the lower part grade upward to very fine to extremely fine tuffs and; 2) a horizontal trend in which the sediments of the lower part of the bed become even coarser towards the southwest and finer tuffs towards the northeast (Fig. 4).

Parallel laminations are more profuse at the coarser-grained base (Fig. 6C) and rare to absent at the fine to very fine-grained top of the bed (Fig. 6D). The laminations are defined by coarser-grained layers enriched in idiomorphic crystals of quartz and plagioclase, interbedded with finer-grained, massive layers mainly composed of homogeneous Y- and cuspate-shaped glass shards. Very rare undulating features resembling current ripples modified by soft-sediment deformation such as load structures have been observed close to the base of the bed. Neither marine fossils nor trace fossils were found, but carbonized wood fragments of up to 3 cm are common throughout the entire bed. The carbonaceous fragments appear in distinctive and irregular layers in close association to medium to coarse pumice lapilli (Fig. 6D). These layers are common near the base and rare in intermediate positions or close to the top of the bed. Some mottling was seen in extremely fine tuffs from the uppermost part (Fig. 6E), where epiclastic and pyroclastic materials were partially mixed.

An up to 0.3 m thick mudstone intercalation is present from Bandurriuas Creek to Guanaquitos Creek (Fig. 6A). It has sharp lower and upper boundaries and wedges out laterally. The tuffs above the muddy intercalation have a coarser-grained base and show an upward-fining (normal grading) trend similar to the tuffs in the lower part of the bed. This grain-size increase is also visible at other localities where the mudstone intercalation is absent (e.g., at Bandurrias Creek South; Fig. 4).

The background sedimentary rocks below and above the LPL are composed of fossiliferous, greenish mudstones and fine-grained sandstones (Figs. 4, 6A), occasionally with levels of spherical carbonate concretions, of 10 to 30 cm in diameter. These sediments were deposited in a low-energy offshore marine environment (Casadío et al., 2000; Cuitiño and Scasso, 2010; Cuitiño, 2011) based on its elevated mud content, high degree of bioturbation and in situ marine fossils.

4.1.2. Upper Pyroclastic Level

The Upper Pyroclastic Level (UPL) is present in the lower part of the continental Santa Cruz Formation, in the transition to the shallow-marine sediments of the underlying Estancia 25 de Mayo Formation. This level is well exposed in the northeastern portion of the area at Estancia Quién Sabe and Los Perros Creek (Fig. 3). This discontinuous bed is composed of a number of lenticular bodies at the same stratigraphic level. The bodies are up to 100 m wide and up to 15 m thick at Los Perros Creek (Fig. 5). Sharp, concave-up bases separate these bodies from the underlying sediments, which vary from mud to fine-grained gravel (Figs. 4, 6E). These characteristics, together with the flat tops, give a general channel-like appearance to these bodies (Fig. 7A).

The pyroclastic bodies are composed mainly of very fine to fine tuffs, with subordinate extremely fine tuffs and medium tuffaceous sandstones. A general coarsening-upward (reverse grading) grain-size trend, from extremely fine tuffs to medium/coarse tuffaceous sandstones is evident for each lenticular body (Fig. 5). In the lower half of the bodies numerous thin lenticular layers composed of flat or elongated pumice particles up to 3 cm in diameter and carbonaceous fragments are present (Fig. 7D), in association with leaf impressions of *Nothofagus* sp. Organic matter from carbonaceous concentrations yielded low

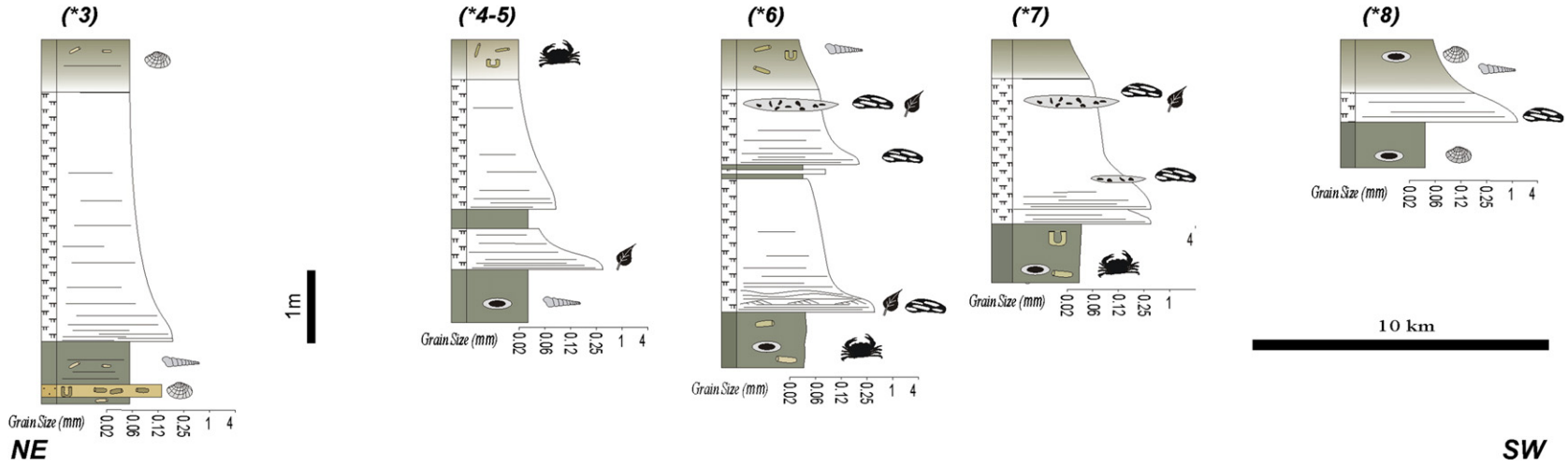

Fig. 4. Detailed sedimentological sections for the LPL including the under- and overlying deposits. Note fining-upward (normal graded) and northeastward thickening trends, as well as dominance of planar lamination and structureless intervals. Numbers above each log indicate its position in Fig. 1B. The LPL is missing at localities *1 and *2. See Fig. 3 for references.

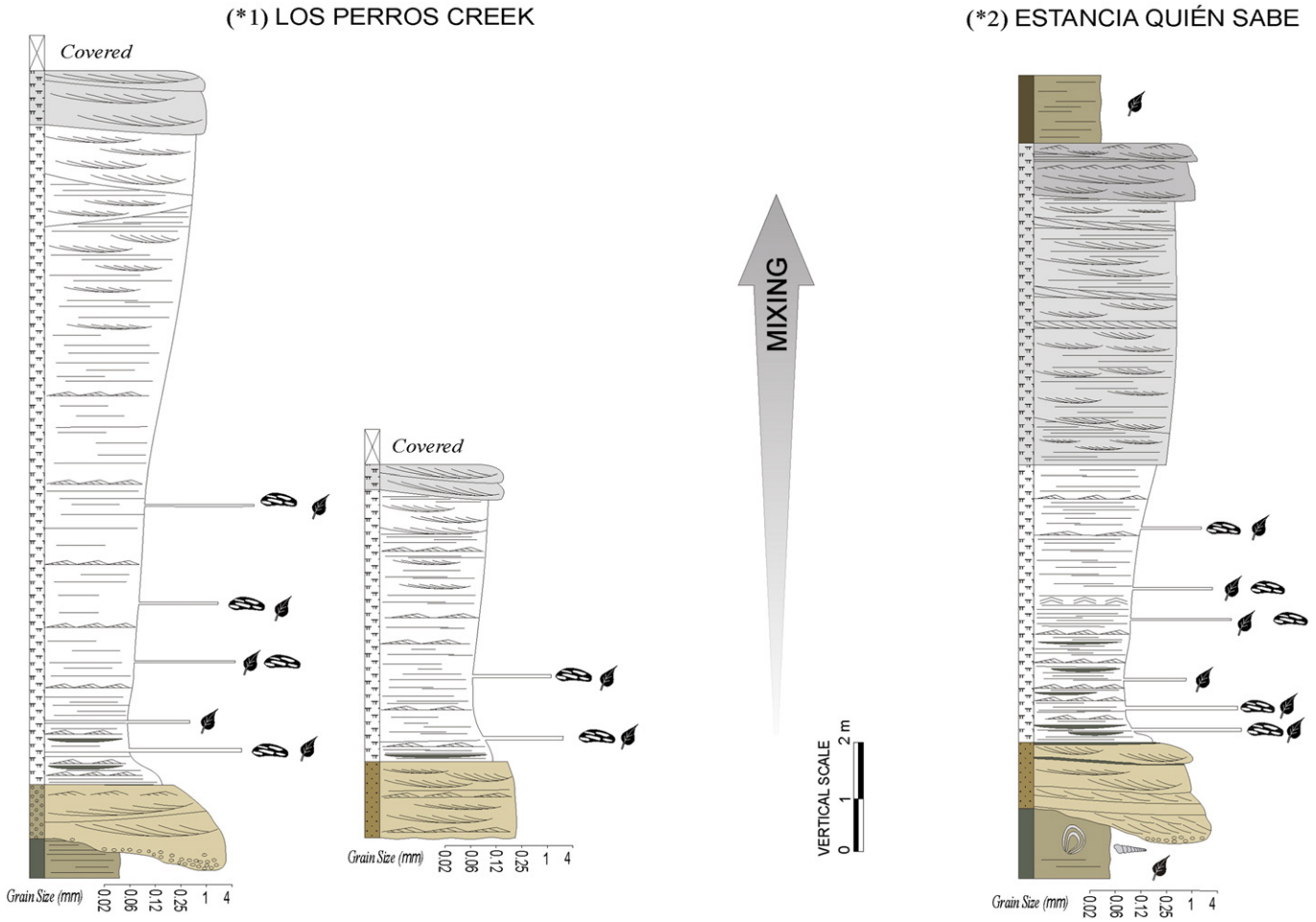

Fig. 5. Detailed sedimentological sections (*1 and *2) for the UPL including the under- and (when preserved) overlying deposits. Note coarsening-upward grain-size and differences in the sedimentary structures between the lower and upper part of the bodies. Shaded areas represent mixed deposits. Both left sections correspond to Los Perros Creek locality. See Fig. 3 for references.

vitrinite reflectance values (around 0.4%) and a TAI of 2 (H. Villar, GeoLabSur, pers. comm., 2009).

Parallel and current-ripple laminations and low-angle cross-stratification are the most common sedimentary structures observed within these bodies (Figs. 5, 7). No massive deposits like those of the LPL were observed. In the lower section, horizontal laminations are dominant, marked by a concentration of heavy minerals or coarse carbonaceous material, normally associated with current-ripple lamination (Fig. 7F). Lenses of a few centimeters thick of light colored mud are intercalated within this lower portion; they are thicker near the base where they form laterally continuous layers. A sharp planar contact separates the lower portion of the body from the upper one, which is formed by slightly darker tuffs and tuffaceous sandstones with larger sedimentary structures such as low-angle and trough cross-bedding in sets of about 15–20 cm thick. Cut-and-fill structures (Fig. 6C) and mud rip-up clasts are common in this portion. The set thickness and angle of trough cross-beds increase toward the top, together with a general increase in grain-size and mixing with epiclastic material (see Section 4.2.2; Figs. 5, 7B).

4.2. Petrographic features

4.2.1. Lower Pyroclastic Level

Thin section analyses reveal that glass (shards + pumice), crystal and lithic particles are the main components of the LPL. The glass fragments exceed 70% of the whole rock, making the shards the dominant component (Fig. 8A–B). The shard proportion varies inversely with the deposit grain-size, with 95% of shards in extremely fine tuffs. Shards are mainly Y- and cuspate-shaped, and some preserve small internal bubbles (Fig. 8B). Shard particle sizes throughout the LPL are variable, from 0.06 mm (extremely fine to very fine tuff; Fig. 8A) to 0.7 mm (coarse tuff). Coarser shards tend to be blocky and show some rounding (Fig. 8B), whereas fine ash tends to be acicular (Fig. 8A). Pumice fragments are abundant in some levels, and dominate in the coarser deposits to the southwest, where shards are nearly absent (Fig. 8C). Isolated, oversized pumice lapilli are common in shard-rich, finer-grained portions. Most vitric particles are devitrified to a mass of very fine-grained crystals (probably quartz and feldspar) arranged in felsitic and rarely axiolitic textures. Few vitric particles are still made of fresh, isotropic glass.

The proportion of crystals is normally less than 10% but increases towards the southwest and reaches up to 20% in the Cuncuna Range. Crystals are generally more abundant in the coarser-grained part near the base. Crystal-size ranges commonly from 0.2 to 0.5 mm (fine to coarse tuff) and decrease from base to top. No horizontal cystal-size variation was recorded. Coarse crystal particles (coarse tuff) show subhedral to euhedral shapes (Fig. 8C), and fine crystals show high angular to acicular shape. Plagioclase is dominant, followed in abundance by quartz, both showing a subhedral shape, vitric rims (Fig. 8C) engulfments and disequilibrium textures (Fig. 8A). K-feldspar, biotite, hornblende, magnetite and rarely pyroxene, garnet, and zircon are also present as accessory minerals.

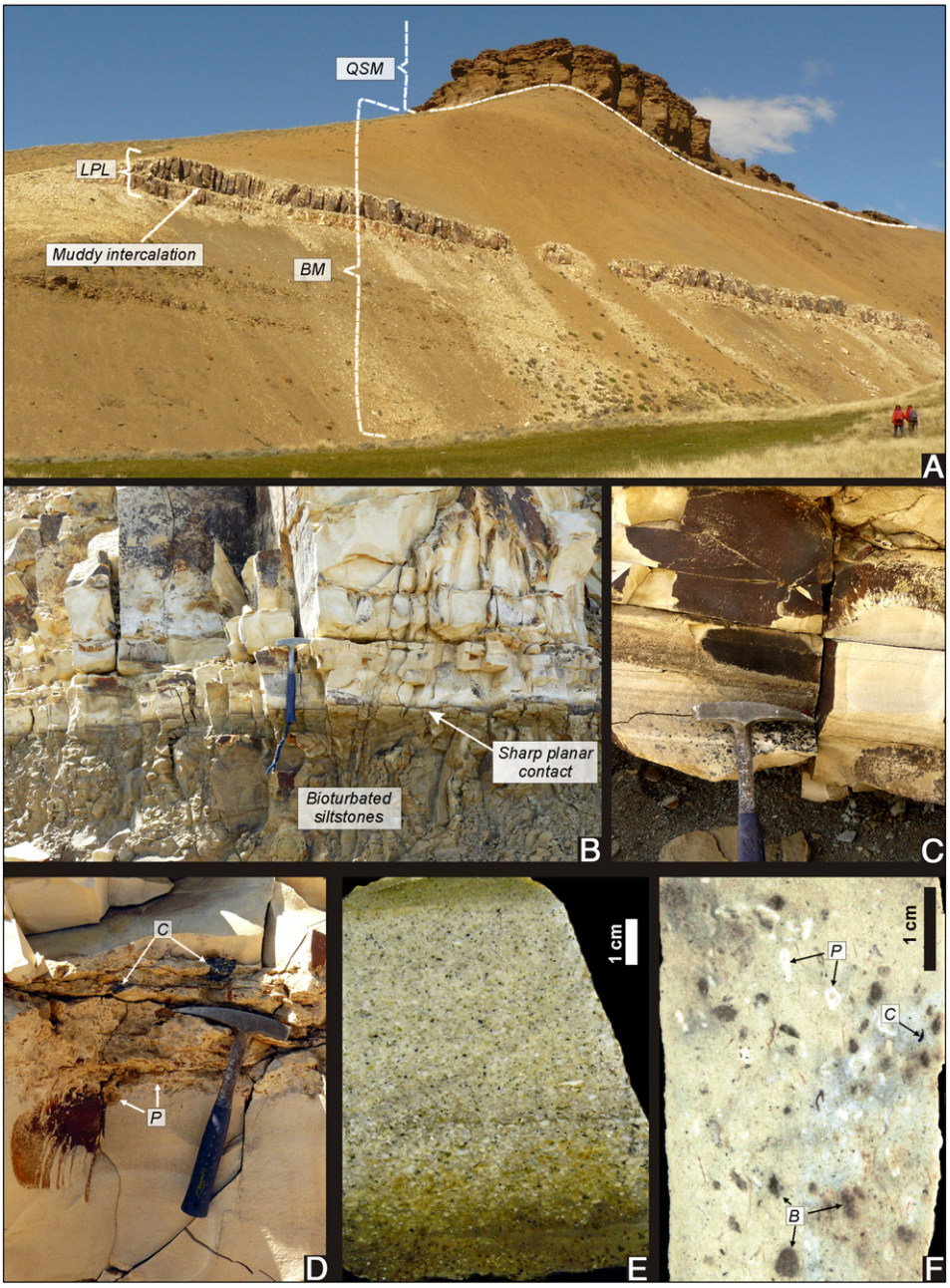

Fig. 6. LPL main features and architecture; A) Panoramic view near Bandurrias Creek locality where the bed is about 3 m thick. Note the tabular shape of the pyroclastic level. BM: mudstones of the Bandurrias Member; QSM: coarse, cross-bedded sandstones of the lowermost part of the Quién Sabe Member. B) Close view of the base at Dos Mellizos Hill. Note the sharp and planar contact above massive and bioturbated siltstones. Layers with diffuse planar lamination are intercalated within structureless very fine tuffs. C) Basal layers at Bandurrias Creek South showing crystal-rich, parallel-laminated medium tuffs. D) Bed showing concentration of large pumice (*P*) and carbonaceous (*C*) fragments, interbedded within massive fine tuffs. Bandurrias Creek South locality. E) Basal layers composed of coarse tuffs with diffuse lamination, dominated by pumice lapilli and crystal particles. Cuncuna Range. F) Extremely fine, massive tuffs from the top of the bed at Bandurrias Creek, showing abundant dispersed pumiceous fragments (*P*), scarce carbonaceous fragments (*C*) and some dark mottles (*B*) interpreted as bioturbation features. Note hammer for scale in those images without a scale bar.

Lithic fragments commonly compose less than 5% of the rock and may be absent in the extremely fine tuffs, but they are more abundant in the coarser-grained parts and reach a maximum of 10% in the Cuncuna Range. They consist mainly of volcanic rock fragments with felsitic or pilotaxitic textures and broken spherulites, with scarce shale or low-grade metamorphic rock fragments.

The deposit was lithified and the porosity obliterated by a brownish to greenish mass of clay-sized minerals probably composed of chlorite, sericite and zeolites diagenetically grown between the clasts. Casadío et al. (2000) mentioned the presence of zeolites detected with XRD analysis. At the Bandurrias Creek locality, calcite patches replacing pumice lapilli fragments are present at the base of the LPL.

4.2.2. Upper Pyroclastic Level

The lower portion of the UPL (Fig. 5) is dominated by very fine-grained vitric material whereas the upper portion shows mixing of coarser pyroclastic and epiclastic material. The boundary between both is marked by a color change and can be sharp (Fig. 7A) or gradual and maybe difficult to recognize in the field.

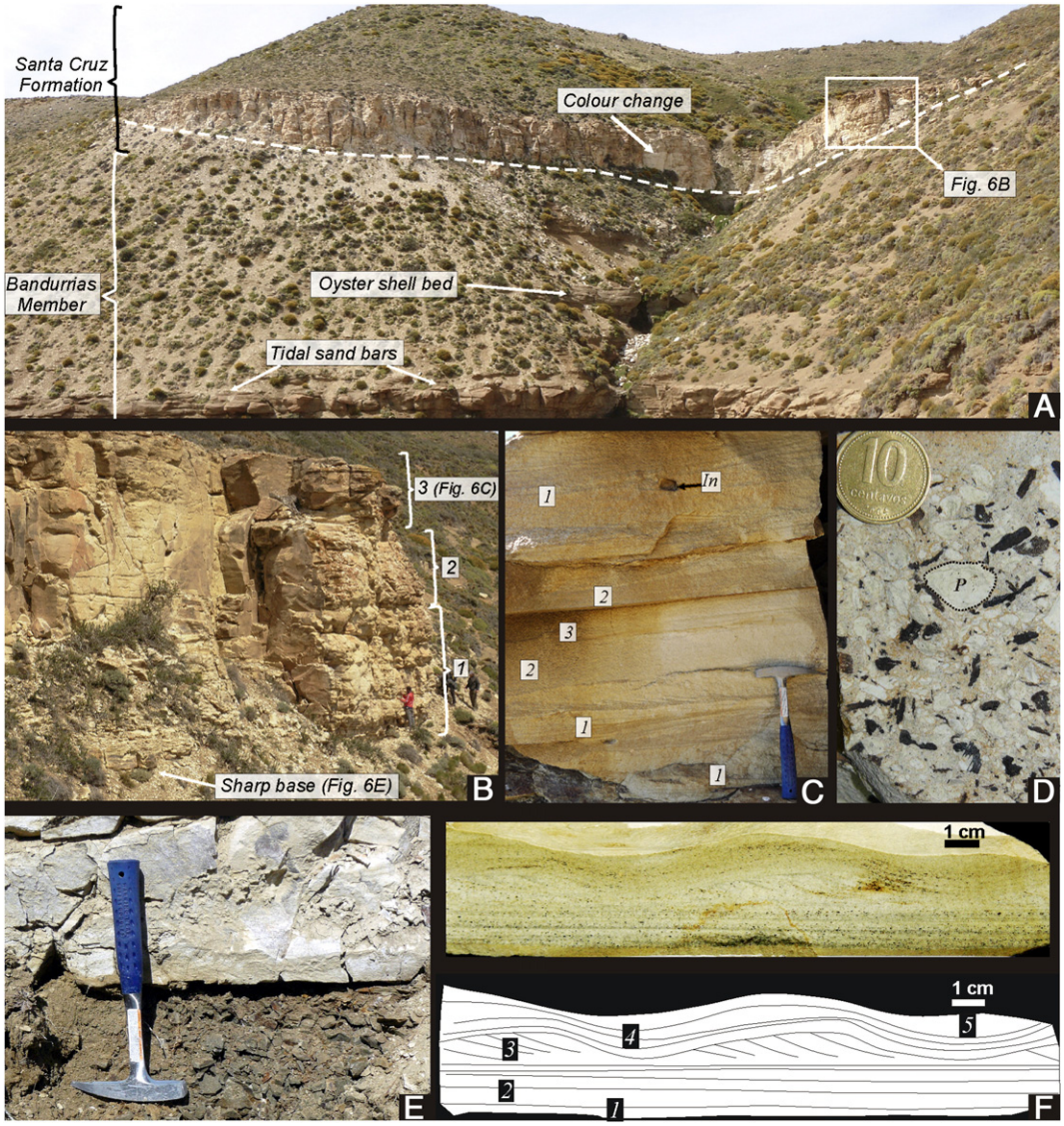

Fig. 7. Architecture and sedimentary features of the UPL. A to E from Estancia Quién Sabe locality and F from los Perros Creek locality. A) Outcrop view of a lenticular body interbedded within the transition from the Bandurrias Member and the Santa Cruz Formation. Maximum thickness is 11 m. Note the arrow in the center of the body indicating a change in coloration, given by a compositional variation. B) Close up view of the body shown in A. Numbers indicate (*1*) the lower very fine-grained tuffs; (*2*) the middle parallel laminated fine to medium tuffs and; (*3*) the upper coarse-grained, cross-bedded tuffaceous sandstones. Persons for scale. C) Sedimentary structures preserved within the upper part shown in Fig. 6B: (*1*) trough cross stratification, (*2*) upper flow regime parallel lamination and (*3*) current ripple cross lamination. (*In*) is a mud intraclast. Hammer for scale. D) Plan view of a layer showing concentration of large pumice (*P*, highlighted) and carbonaceous (dark) fragments. A coin (1 cm in diameter) for scale. E) Base of the body showing a sharp contact between very fine to extremely fine tuffs (whitish) overlying dark massive mudstones. Hammer for scale. F) Polished hand sample showing small-scale sedimentary structures representing a short-lived waning flow. At the base a flat extremely fine tuff layer (*1*), followed by medium tuffs with UFR parallel lamination (*2*), medium to fine tuffs with current ripple cross-lamination (*3*), fine tuffs with climbing ripple lamination containing carbonaceous chips (*4*) and finally a layer of extremely fine tuff blanketing the ripple forms (*5*).

Glass particles in the lower portion form 75% to 95% of the whole rock (Fig. 8D). Finer-grained particles are made up mainly of vitric shards (normally 0.1 mm; very fine tuff) with platy to Y shapes, whereas coarser ones are made of pumice lapilli. Few interbedded thin layers rich in carbonaceous fragments and pumice particles of up to 1 cm are present (Fig. 7D). Crystal particles (mean 0.1 mm; very fine tuff) are concentrated in millimeter-thick layers, mainly composed of plagioclase and quartz, with subordinate biotite, K-feldspar, and minor hornblende, pyroxene, zircon, and garnet. They show highly angular shapes and form about 10% of the fine-grained sections (Fig. 8D), whereas coarse-grained and parallel laminated layers contain about 25% of crystals. Rare, lithic particles are dominated by volcanic fragments with felsitic textures, although fragments of shale, low-grade metamorphic or basic volcanic rocks can also be present.

The upper portion of the pyroclastic bodies shows parallel lamination in the medium to coarse tuffs and decimeter-scale cross-bedding in the tuffaceous sandstones. Pumice-dominated layers intercalate with crystal- or lithic-dominated layers (Fig. 8F). Coarse pumice fine- to medium-lapilli fragments can compose up to 95% of the rock. Unlike the pumiceous layers of the lower portion, these pumiceous layers are laterally continuous, finer-grained (mean 0.8 mm) and display a grain size similar to the surrounding sediments (Fig. 8E). Vesicles within pumice particles are elongated and parallel each other, but show a random orientation in relation to rock lamination. Glass shards are uncommon and the proportion of lithic particles is overall higher in this portion, reaching up to 50% of the rock in some layers. The lithic clasts comprise mainly volcanic fragments with dominant mafic and minor felsitic textures (Fig. 8E), which give a darker color to the sediments (see detail in Fig. 7A). In addition, low-grade metamorphic and silty

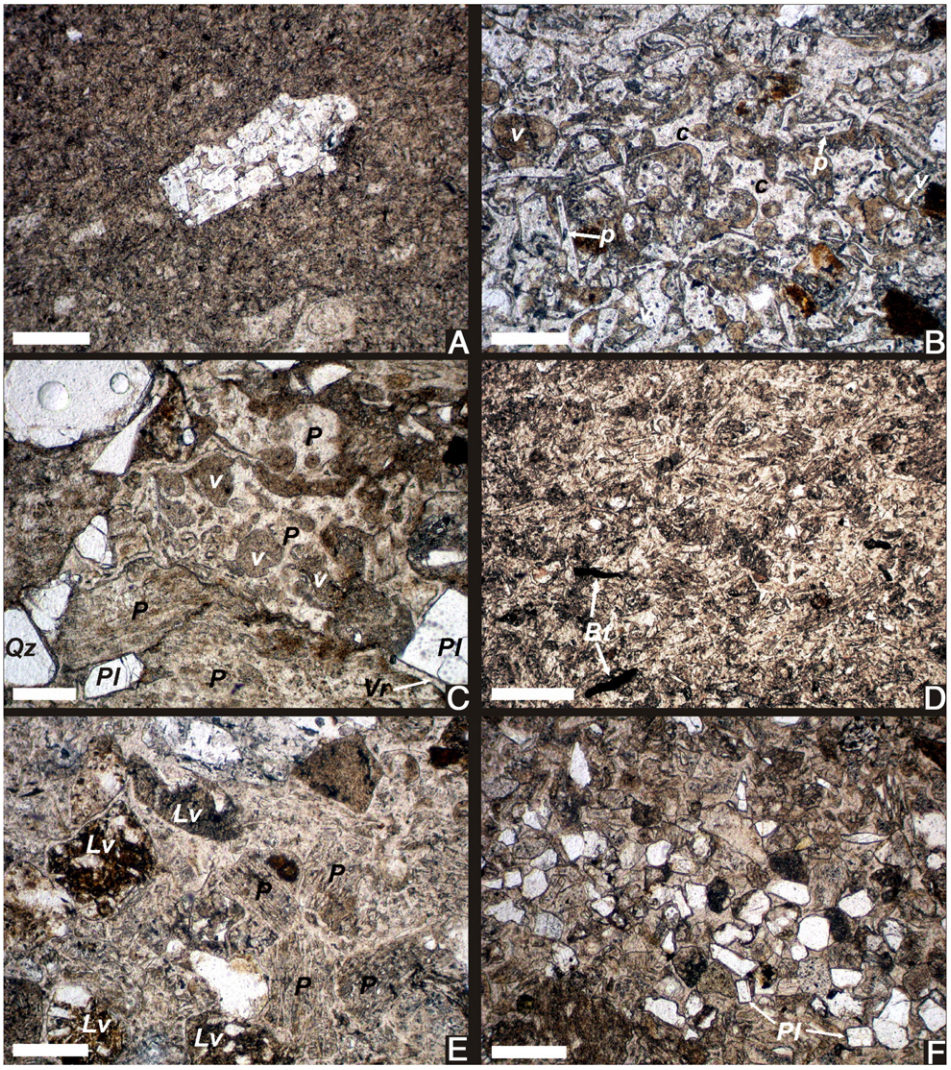

Fig. 8. Petrographic features of the pyroclastic levels. Scale bar 0.5 mm. Plane-polarized light. A) Very fine tuffs composed almost entirely by vitric shards. A plagioclase phenocryst in the center with glassy remains of adhered bubble walls and corrosion textures. Base of the LPL at Estancia 25 de Mayo. B) Fine to medium tuff composed by large vitric shards. Cuspate (*c*) to platy (*p*) forms with incipient rounding are common. Brownish material, sometimes filling the vesicles (*v*), is composed of very fine-grained clay minerals. Base of the LPL at Bandurrias Creek locality. C) Coarse, pumiceous and crystal-rich tuff. Large pumice lapilli fragments (*P*) showing vesicles (*v*). Crystals are plagioclase (*Pl*) and quartz (*Qz*). Base of the LPL at Cuncuna Range. Note the increase in grain size from A to C. D) Vitric, shard-dominated, very fine tuff from near the base of a body at Estancia Quién Sabe. Shards show platy and acicular shapes. Crystals (mainly *Qz*) are scarce and very fine-grained. Some dark oxidized biotite flakes (*Bt*) are present. E) Tuffaceous sandstone with elevated proportions of mafic volcanic lithic (*Lv*) fragments. Note the absence of glass shards and the abundance of pumice (*P*) particles. Upper portion of the UPL at Estancia Quién Sabe. F) Tuffaceous sandstone showing a layer enriched in crystal particles, mainly of angular/subangular quartz and subhedral plagioclase (*Pl*). Top of the UPL at Los Perros Creek.

rock fragments are present. Crystals (5%–25%) are dominated by angular quartz and euhedral plagioclase (Fig. 8F), with a lower proportion of deformed biotite flakes, feldspar, hornblende, clinopyroxene, and magnetite.

A very fine-grained, translucent, and low-birefringence matrix probably composed of clays and zeolite minerals, fills the vesicles and pores, reducing the porosity to near zero.

5. Geochemistry

Bulk-rock chemical analyses (Table 2) of major elements were made on six samples (three samples per level) showing negligible mixing with epiclastic material. Samples of the UPL were taken from the tuffs in the lower part of the bodies, where the silica content varies from 62% to 74%. Samples from the LPL are more silicic than those from the UPL (sample AB-V yielded low SiO_2, but this could be the result of diagenetic replacement of SiO_2 by $CaCO_3$). In a total-alkali-silica (TAS) diagram (Fig. 9), all the samples plot in the dacite field, although those from the LPL are close to the rhyolite boundary, whereas those from the UPL are close to the andesite boundary. The absence of mixing with epiclastic sediments suggests that the composition of the silicic magma may be coeval or genetically related with the magma responsible for the Southern Patagonian Batholith (Hervé et al., 2007; see Section 7 for further details).

6. Interpretation of ash sedimentation/preservation processes

The sedimentary, petrographic, and geochemical characteristics, together with the close temporal affinities between these two pyroclastic levels, suggest that both could have a similar volcanic source. However, their different modes of preservation reveal the influence of sedimentary environments on the final nature of the deposits,

Table 2
Bulk-rock chemical composition, recalculated to oxides, of three samples per pyroclastic level. Methods used for analysis are described in Section 5. Shaded results for ABV correspond to anomalous values caused by diagenetic carbonate precipitation.

Sample		SiO_2	TiO_2	Al_2O_3	Fe_2O_3	MnO	MgO	CaO	Na_2O	K_2O	P_2O_5	CO_2	H_2O^+	H_2O^-	Sum
UPL	Toba 4	63.22	0.16	13.89	1.32	0.03	1.96	2.72	2.20	0.91	0.03	–	7.27	5.52	99.23
	Toba 5	62.97	0.25	14.44	1.88	0.01	1.48	3.31	2.84	0.99	0.03	–	5.88	5.26	99.35
	ALPX	64.32	0.20	12.96	1.63	0.02	1.67	3.34	2.60	1.20	0.03	–	5.84	5.18	99.00
LPL	LS 17	71.84	0.17	10.76	0.32	0.02	1.75	3.21	1.73	0.64	0.02	–	4.77	3.84	99.06
	Cuncuna	74.12	0.31	8.27	0.83	0.03	1.83	4.21	2.06	0.67	0.03	–	4.21	3.55	100.12
	ABV	56.31	0.16	12.89	1.20	0.02	2.23	8.01	1.72	0.89	0.02	6.66	5.74	4.96	100.82

and in turn, the strong influence that explosive volcanism had over the sedimentary systems and their dynamics.

6.1. Origin of the Lower Pyroclastic Level

The enclosing sediments of this pyroclastic unit are homogeneous, massive and poorly stratified, fully bioturbated siltstones, showing a rich and diverse invertebrate fauna, including many genera of bivalves, crustaceans, gastropods and echinoderms. These features suggest a well oxygenated and normal-salinity marine environment with limited wave or tidal currents influence, in a low-energy offshore marine setting during the transgressive phase of the *Patagoniense* transgression (Cuitiño and Scasso, 2010; Cuitiño et al., 2012). In the north-eastern part of the study area the LPL is not preserved. There, the presence of storm levels represented by coarse-gained facies, erosion surfaces and reworked shell beds (Fig. 3), suggests the possible erosion of the LPL under shallower-water conditions.

The tabular shape and lateral extension (at least 30 km) of the LPL, together with the small variations in grain size, reflect smooth sea-bottom topography and similar sedimentation conditions at the moment of deposition of the pyroclastic material on this, which blanketed the paleosurface. In this low-energy context, the pyroclastic particles, supplied by the explosive volcanism, reached the sea bottom either by direct ash fallout and subsequent decantation in the marine basin or by fluvial input at coastal settings and redistribution to the deeper part of the sea floor, and then were preserved without subsequent reworking. This implies that bioturbation must be hindered during and shortly after the deposition of the pyroclastic bed, since no trace fossils were observed, excepting to the uppermost part. The grain-size distribution throughout the pyroclastic body shows the dominance of angular, very fine to fine ash particles, except for the coarser basal layers and the pumiceous intercalations (Fig. 4). Dominance of glass shards, angular particles and normal grading, together with the large areal extent of the pyroclastic deposit, are patterns similar to that observed for submarine pyroclastic fallout deposits, where coarser material settles earlier to the depositional site, followed by the fine pyroclastic dust (Sigurdsson et al., 1980; Wiesner et al., 1995). Direct fallout trough the water mass or, more recently, diffuse vertical gravity currents (Carey, 1997) are the suggested depositional mechanisms. However, the great thickness of the LPL (up to nearly 4 m) challenges this interpretation since air fall-out deposits on the sea floor are hardly thicker than a few centimeters (Sigurdsson et al., 1980; Bonadonna et al., 1998; Wiesner et al., 2004; Wetzel, 2009). Even in areas less than 30 km away from the eruption site, ash-fall deposits rarely are more than a few decimeters thick (Bonadonna et al., 1998) and typically are characterized by a large grain size of 4–8 mm on average (Lirer and Vinci, 1991). The LPL deposits range in thickness from 0.3 to nearly 4 m and their grain-size is mostly in the 0.1–0.3 mm range. Processes such as wave or tidal action would have resulted in mixing of the pyroclastic and epiclastic particles, and a better rounding of the former. Therefore, direct air fallout cannot be responsible for the concentration of the ash in this submarine environment. Sigurdsson et al. (1980) arrived at a similar conclusion when describing modern ash layers preserved in the bottom sediments of the Caribbean Sea. These authors interpreted decimeter thick, well-sorted ash beds as deposits from sediment gravity flows, whereas direct fallout processes are represented by massive ash layers of a few centimeters thick. Additionally, some rounding of coarse glass particles suggests reworking of the highly-angular primary pyroclastic material (Fig. 8B, compare with Carey et al., 2000).

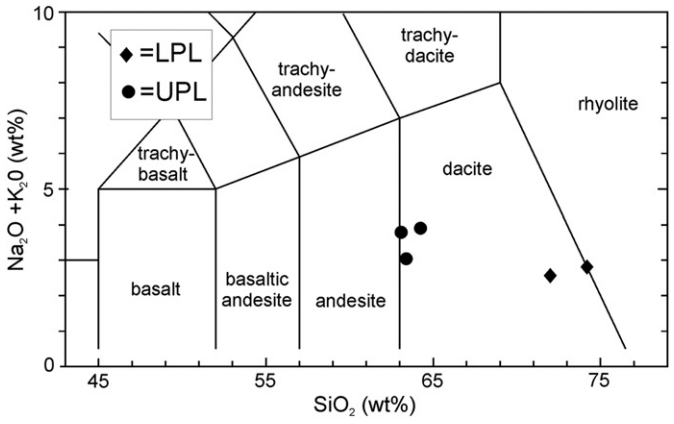

Fig. 9. Total alkali-silica (TAS) diagram with defining fields from Le Bas et al. (1992). Lower dacite almost andesite area for the UPL samples, and upper dacite area for the LPL samples.

Hyperpycnal flows can occur in marine coastal environments associated with volcanic eruptions, such as the jökulhlaups in Iceland (Mulder et al., 2003). They originate where a river in flood enter a standing body of water (typically the ocean, or lakes) carrying large amounts of sediment in suspension (Mulder et al., 2003), a common condition during explosive volcanic eruptions. These sediment-laden flows can exceed the density of marine waters and plunge into the sea, flowing and transporting material over the basin floor for large distances (up to 70 km; Mulder and Syvitski, 1995; Mulder et al., 2003; Zavala et al., 2010). The minimum suspended-load concentration to surpass marine-water density varies from 35 to 45 kg/m^3 (Mulder and Syvitski, 1995). For example, the 1991 eruption of Mount Pinatubo increased the suspended load concentration of nearby rivers up to 290 kg/m^3 (Hayes et al., 2002). Additionally, it has been suggested that the ability of river discharge to generate hyperpycnal flows could be enhanced in mountainous rivers draining small basins (Mulder and Syvitski, 1995; Mulder et al., 2003). This appears to be the case for the

LPL, considering that the *Patagoniense* transgression reached the foothills of the active volcanic Andean ranges, thus leaving a reduced subaerial region in areal extent (about 100–150 km wide) with rivers draining small watersheds, favoring the formation of hyperpycnal flows (Mulder and Syvitski, 1995).

The grain-size of deposits produced by hyperpycnal flows varies from gravel to mud, where bedload, suspended load, and lofting-related facies were defined as part of a general genetic model (Zavala et al., 2010). The grain-size of the LPL is predominantly within the fine sand to silt range as the particles produced by the explosive eruption were originally fine-grained. In addition, sorting during fluvial transport would have preferably removed the coarser particles. The LPL is dominated by structureless fine tuffs, and some parallel laminated fine to medium tuffs are present mainly near the base of the unit. Meter-thick structureless deposits are a frequent product of hyperpycnal flows (Kneller and Branney, 1995; Zavala et al., 2010). Massive or diffuse laminated sands form because tractional structures are prevented by the absence of a sharp rheological interface between the lowest parts of the flow and the just-formed deposit (Arnott and Hand, 1989), resulting in elevated rates of aggradation by a heavy rain of sediment from the turbulent suspension (Kneller and Branney, 1995; Sumner et al., 2008). The basal layers comprise coarse, crystal-rich tuffs with parallel lamination that can be explained by segregation of heavy particles (crystals) due to frictional forces over the bed at initial flow stages. These basal layers dominate in the southwest and show a lateral fining trend to the northeast, indicating a preferential deposition of coarse and heavy material near the source of the hyperpycnal flow (Fig. 10). A thick succession of massive or poorly laminated fine tuffs overlies the thin basal layers. Neither an erosional nor a sharp contact exists between both parts, possibly related to a gradual change from bedload to suspended-load processes (cf., Zavala et al., 2010). The upper portion of the level also shows a fining trend to the northeast, and thickens in the same direction. These fine-grained layers show a concentration of carbonized wood remains and large pumice lapilli fragments near the top, which are interpreted as the result of lofting of the lighter material together with the freshwater supplied by the river, which is deposited at the final stages of the flow movement (Zavala et al., 2010). The presence of coarse carbonaceous plant fragments supports the interpretation that the material was directly supplied from land (Mulder and Alexander, 2001; Plink-Björklund and Steel, 2004; Zavala et al., 2012). These volcanic events largely affect the subaerial vegetation, producing high amounts of vegetal debris that finally are incorporated into the fluvial systems as the result of post-eruption runoff. During early Miocene times, the Andean Patagonia was covered by a Nothofagus forest similar as today (Barreda and Palamarczuk, 2000), thus volcanic activity may have seriously damaged the vegetation cover. Modern examples such as the 2008 eruption of the Chaitén volcano (Alfano et al., 2011) and the 2011 eruption of the Puyehue-Cordon Caulle serves as analogs.

The great thickness and large areal extent of the LPL point to a long-lived source of underflows or sustained turbidity currents that could last days or weeks (Mulder et al., 2003; Plink-Björklund and Steel, 2004). The mudstone intercalation seen in some localities suggest periods of low activity followed by new increments in flow power evidenced by grain-size reactivations. This phenomenon is probably related to pulsatory, heavy rainfall events in the continent that washes the already deposited pyroclastic material into the rivers.

Ash layers deposited in marine settings usually show profuse bioturbation and in many cases are completely mixed with surrounding sediments (Sigurdsson et al., 1980; Wetzel, 2009). In our case, the pyroclastic deposit is barren of bioturbation or any marine body fossil with the exception of few small biogenic structures affecting the uppermost layers at Bandurrias Creek section. Very high sedimentation rates, relative to the background rate for the epiclastic regime, combined with the input of freshwater carried by the flows, suggest highly stressful conditions for benthic communities living within the basin (Buatois et al., 2010). An additional source of stress may be the acidification of the flowing water caused by the interaction of the volcanic particles with the surrounding water.

6.2. Origin of the Upper Pyroclastic Level

Sediments below and above this level are massive or diffusely laminated mudstones and coarse-grained sandstones with few interbedded fine-grained conglomerates, showing plant and mammal remains,

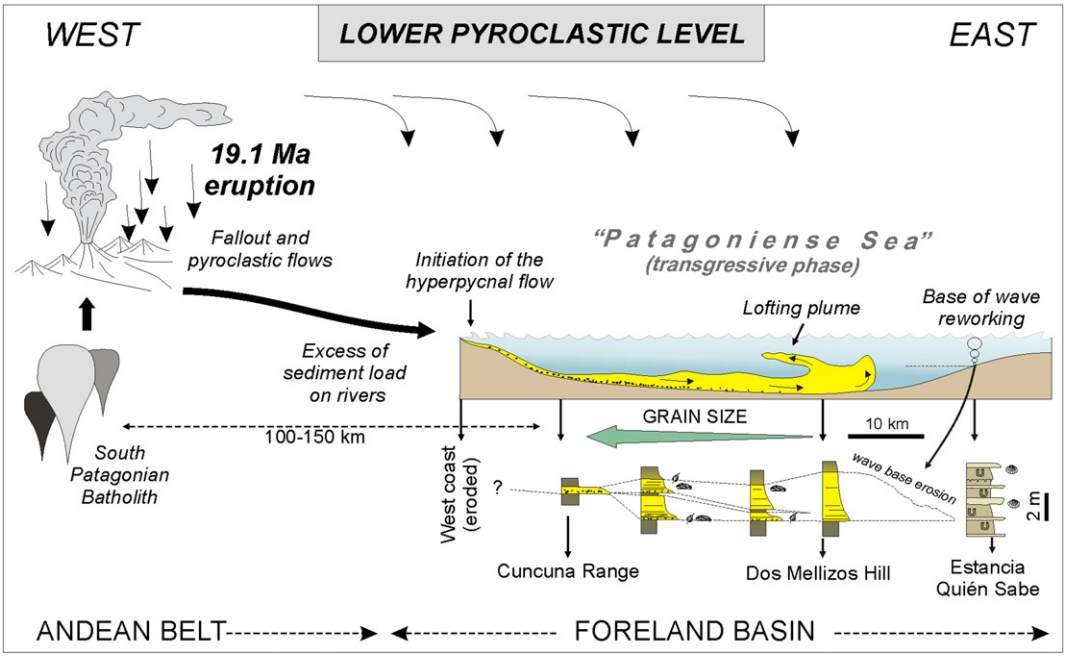

Fig. 10. General model for the deposition of the LPL.
Distances from source area are based on data from Hervé et al. (2007).

suggesting a terrestrial environment. These epiclastic sand bodies, with sharp erosional bases and a fining-upward trend, are interpreted as the infilling of fluvial channels, whereas the muddy portion corresponds to adjacent floodplains. In this stage a normal regression of the shoreline cause the shallow marine environment to gradually shift to a coastal alluvial plain network. The dominance of mud over the sand bodies, in combination with the close relationship with underlying estuarine sediments, suggests a low-energy fluvial environment draining a low-gradient coastal/delta plain (Fig. 11A). The small lateral extension of the preserved sand bodies suggest that they may have accumulated from low-sinuosity fluvial channels (Gibling, 2006). The UPL is composed of a number of small lenticular bodies showing concave up, erosive bases and plane tops, interpreted as the pyroclastic infill of fluvial channels. The pyroclastic material is preserved only inside the channels and no discrete pyroclastic bodies were observed interbedded within floodplain deposits. The width to height ratios of these bodies are low (6 to 10) and can be classified as "broad ribbons", which are channels showing no or little lateral migration and rapid filling (Gibling, 2006). The sudden infill of the channels by rivers overloaded with pyroclastic sediments mimics their shape at a given, nearly instantaneous point in time, therefore preventing the lateral migration process that should be evident in the adjacent epiclastic deposits. Unfortunately, poor exposure of the nearby deposits (Fig. 7A) precluded further exploration of this hypothesis. Mixing of the pyroclastic and epiclastic particles has not been recognized in the basal layers of the pyroclastic bodies, suggesting that during the infilling the normal conditions of fluvial streams were deeply modified. Sudden deposition of material may have triggered rapid channel fill and abandonment of the lower portion of the bodies.

Upper flow regime parallel lamination and cross-lamination indicate tractive currents. Current ripples preserved as bedforms in the bedding planes with ripple indexes of 6 to 7 indicate that these are subaqueous deposits (Tanner, 1967). The associated intercalated muddy layers are the result of slack-water (low-energy) episodes. Neither desiccation cracks nor other features considered typical of subaerial exposure are present. A pyroclastic flow origin of these deposits is disregarded since the carbonaceous fragments indicate that carbonization could be the result of diagenesis and not of high-temperature burning during the eruption. Organic matter from adjacent muddy layers shows similar preservation conditions as the carbonaceous fragments from the pyroclastic level (H. Villar, personal communication, 2009). All these features indicate that the pyroclastic deposit is the result of deposition by fluvial streams.

All channelized pyroclastic bodies show a coarsening upward (reverse graded) trend, opposed to the classic model for the filling of fluvial channels (Miall, 1996). The lower portion consists mainly of parallel laminated, very fine-grained vitric tuffs (from 0.03 to

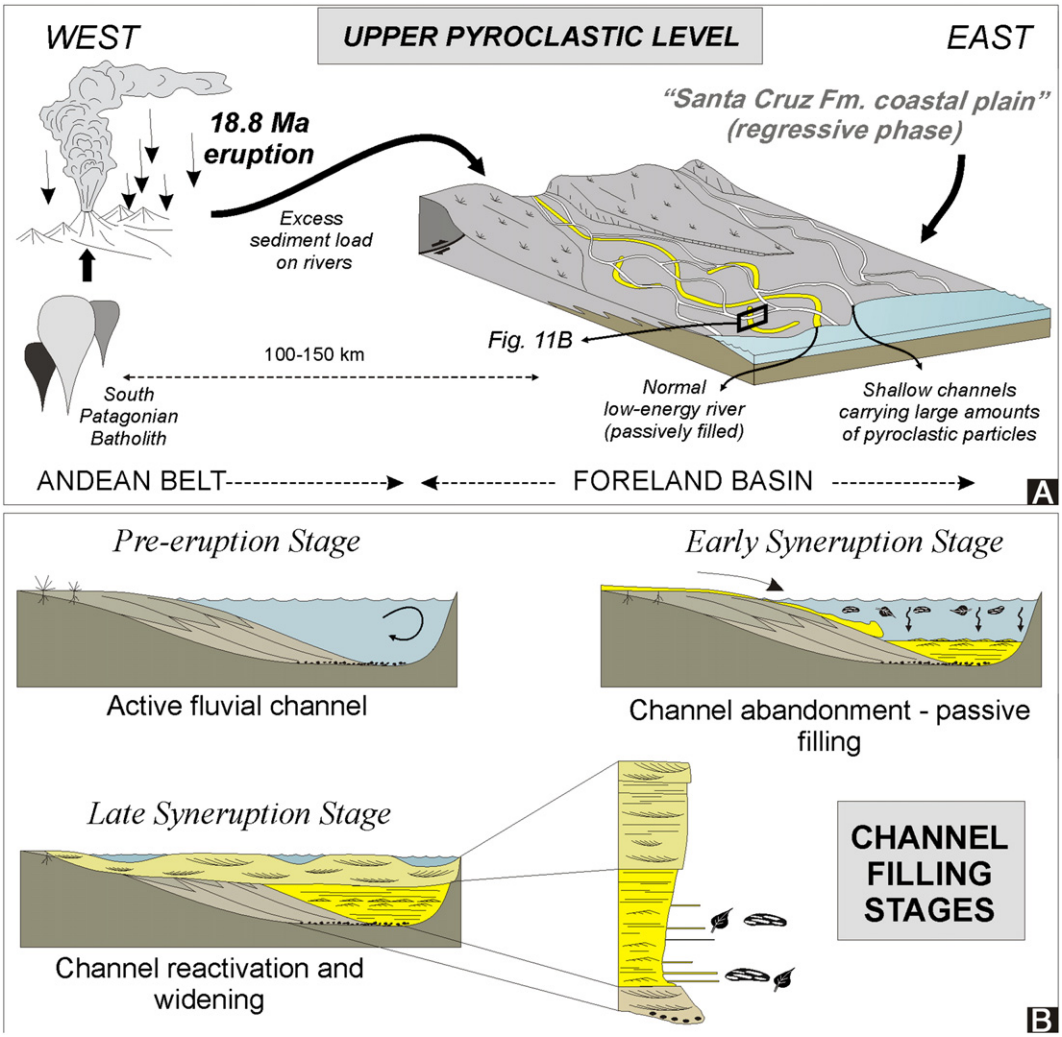

Fig. 11. General model for the deposition of the UPL. A) Yellow streams indicate original fluvial style. White streams indicate reactivation and modification of the fluvial drainage. Location of B is indicated within the coastal plain. B) Detail of three stages of pyroclastic infilling of the fluvial channels in the coastal plain.

0.13 mm) interpreted as formed in the upper flow regime, with an upward gradation to current-ripple lamination and finally to mud drapes, forming cycles of decreasing flow energy (Fig. 7F). These features, plus the presence of frequent mud intraclasts, indicate fast and short-lived flows that wane recurrently and stopped their motion giving place to the normal background sedimentation in a low-energy environment. Small lenses showing concentration of pumice lapilli and abundant carbonized vegetal fragments (Fig. 7D) also support the occurrence of slack-water periods as well as the evidence for widespread vegetal cover destruction during the eruption. The absence of scouring in this part of the bodies suggests elevated sedimentation rates given by sediment-laden flows which not were able to erode the substrate.

The upper portion of the lenticular bodies is dominated by coarse-grained tuffs or tuffaceous sandstones (from 0.25 to 2 mm) showing trough cross-bedding and cut-and-fill structures. These, together with the increasing degree of mixing of pyroclastic/epiclastic material, reflect the capability of streams to erode the substrate, related to a decrease in the amount of sediment load in the water flowing through the channels. Additionally, the lateral extension of these upper tuffaceous sandstones is higher in relation to the lower portion, indicating widening of channels, possibly by shallow braided streams (Fig. 11B).

Explosive volcanic eruptions supply catastrophic amounts of sediment into the neighboring basins, causing the streams to quickly fill, avulse and reduce their sinuosity (Smith, 1991). Fast aggradation of the channel beds and subsequent shift in their positions can occur during explosive eruptions (Kuenzi et al., 1979; Smith, 1991; Hayes et al., 2002; Alfano et al., 2011). The lack of mixing in the lower layers indicates that the transport capacity of the streams was overcome. Rivers draining recent volcanic regions from Guatemala transported sediments loads with 95% pyroclastic-derived material (Kuenzi et al., 1979). The main source of pyroclastic particles carried by fluvial streams comes from the erosion of loose, tephra fallout deposits that mantle the surface in proximal to distal areas of the volcanic vent (Major et al., 1996), yielding a huge amount of fine grained particles to the catchment areas.

The slack-water evidence indicates that the channels were occupied, at least at the initial stage of pyroclastic deposition, by a semi-standing body of water, suggesting that the channel was partly abandoned and quickly filled by short-lived, repetitive flows (Fig. 11B). These initial flows can be interpreted as small hyperpycnal flows generated during the supply of sediment-laden flows that fed the channel scour. Evidence for slack-water decreases upward, being replaced by parallel and current ripple laminated tuffs, indicative of the arrival of sandy sheetflood deposits in shallower water. Finally, stronger and deeper currents produced large-scale bedforms and partially remobilized the underlying sediments, thus producing cut and fill structures, widening of the upper portion of the channel and mixing with epiclastic material, culminating the coarsening upward trend for the infill of the fluvial channel (Fig. 11B). Similar prograding patterns were described for the infilling of abandoned channels by Gilbert-type deltas during explosive volcanic activity in the modern pacific coastal plain of Guatemala (Kuenzi et al., 1979).

The lack of discrete, tabular pyroclastic layers in the adjacent flood-plain deposits suggests that ash fallout did not occur in this area, probably because of an unfavorable wind direction during the eruption.

7. Source of pyroclastic material

The lateral coarsening westward trend observed throughout the LPL indicates that the feeding of the hyperpycnal system was located to the west or southwest, in coincidence with the position of the palaeocoastline for the early Miocene (Cuitiño, 2011). This coastline received the discharge of fluvial streams that drained catchment areas coming from the Patagonian Andes, where magmatism was common during early Miocene times (Hervé et al., 2007). The pyroclastic material analyzed here is contemporaneous with a magmatic pulse of the South Patagonian Batholith (Hervé et al., 2007). There, a number of early Miocene intrusive bodies of tonalite–granodiorite composition were identified (Hervé et al., 2007). Considering the age obtained for the pyroclastic levels, around 20–19 Ma for the LPL and 18.8 Ma for the UPL (Cuitiño et al., 2012), some plutons of similar ages and proximal geographic location can be related. In the same age range (from 18 to 21 Ma), six intrusive bodies ranging from tonalites to granites are present in a region from 90 to 170 km west of the study area (Hervé et al., 2007). The intermediate to silicic composition of the magmas suggest that these plutonic bodies could represent the chambers that fed the explosive eruptions that supplied the pyroclastic material to the adjacent foreland basin.

8. Conclusions

Supply of large amounts of pyroclastic particles to the early Miocene sedimentary systems of the Austral Basin is well recorded in two major pyroclastic levels that were preserved in different sedimentary environments showing disparate modes of preservation, and providing a good example for analyzing how sedimentary environments react to the catastrophic supply of sediments during explosive volcanic eruptions.

The tabular LPL is interpreted as the result of hyperpycnal flows generated at the mouth of rivers carrying large amounts of fine grained pyroclastic particles that by-passed the nearshore area and reached the sea bottom. No erosive surfaces at the interior or top of the body were found suggesting deposition well below the wave base, allowing all the deposited material to be finally preserved. Such a situation was favored by the phase of high relative sea-level in the *Patagoniense Sea*, which brought the coastline into a closer (western) position in relation to the inferred volcanic source.

In contrast, the UPL shows a discontinuous lateral arrangement of lenticular bodies that are interpreted as the infill of fluvial channels. The progradational pattern for the infill represents initial frequent and short episodes of slack water, with partial abandonment of the channels, leaving place to small stagnant water bodies. The available space was quickly filled by short-lived bottom flows, interpreted as hyperpycnal flows created by small streams feeding the abandoned channel. Shallow streams with the capability to erode the substrate and cut banks produced channel reactivation, widening, and deposition of cross-stratified tuffaceous sandstones in the upper part of the UPL. This fluvial behavior is common in modern volcanic systems (Kuenzi et al., 1979).

Grain-size, geochemical, and petrographic similarities between both levels suggest they were probably sourced by the same volcanic complex, located along the axis of the present day South Patagonian Batholith. The eruptions suddenly overloaded the sedimentary system and deeply modified the transport-deposition dynamics. Both pyroclastic levels represent different distal expressions of a volcanically-influenced sedimentary system.

Acknowledgments

This research was funded by the Universidad de Buenos Aires, CONICET and ANPCyT (PICT 25342) of Argentina. We are grateful to Héctor Villar (GeoLab Sur) for organic matter analyses. David Kratzmann and Steven Carey provided valuable suggestions and language corrections of early versions of the manuscript. Thorough reviews by Károly Németh and Carlos Zavala, as well as suggestions by Editor Gert Jan Weltje, contributed significantly to the improvement of the final manuscript.

References

Alfano, F., Bonadonna, C., Volentik, A.C.M., Connor, Ch.B., Watt, S.F.L., Pyle, D.M., Connor, L.J., 2011. Tephra stratigraphy and eruptive volume of the May, 2008, Chaitén eruption, Chile. Bulletin of Volcanology 73, 613–630.

Arbe, H.A., 2002. Análisis estratigráfico del Cretácico de la Cuenca Austral. In: Haller, M.J. (Ed.), Geología y Recursos Naturales de Santa Cruz. Relatorio del XV Congreso Geológico Argentino: El Calafate, I-8, pp. 103–128.

Arnott, R.W.C., Hand, B.M., 1989. Bedforms, primary structures and grain fabric in the presence of suspended sediment rain. Journal of Sedimentary Petrology 59, 1062–1069.

Barreda, V.D., Palamarczuk, S., 2000. Palinomorfos continentales y marinos de la Formación Monte León en su área tipo, provincia de Santa Cruz, Argentina. Ameghiniana 37, 3–12.

Barreda, V.D., Palazzesi, L., Marenssi, S., 2009. Palynological record of the Paleogene Río Leona Formation (southernmost South America): stratigraphical and paleoenvironmental implications. Review of Palaeobotany and Palynology 151, 22–33.

Bellosi, E.S., 1995. Paleogeografía y cambios ambientales de la Patagonia central durante el Terciario medio. Boletín de Informaciones Petroleras 44, 50–83.

Biddle, K.T., Uliana, M.A., Mitchum Jr., R.M., Fitzgerald, M.G., Wright, R.C., 1986. The stratigraphic and structural evolution of the central and eastern Magallanes Basin, southern South America. In: Allen, P., Homewood, P. (Eds.), Foreland Basins. Special Publication, 8. International Association of Sedimentologists, pp. 41–61.

Bonadonna, C., Ernst, G.G.J., Sparks, R.S.J., 1998. Thickness variations and volume estimates of tephra fall deposits: the importance of particle Reynolds number. Journal of Volcanology and Geothermal Research 81, 173–187.

Buatois, L.A., Saccavino, L.L., Zavala, C., 2010. Ichnologic signatures of hyperpycnal-flow deposits in Cretaceous river-dominated deltas, Austral Basin, Southern Argentina. In: Slatt, R.M., Zavala, C. (Eds.), Sediment Transfer From Shelf to Deep Water—Revisiting the Delivery System: AAPG Studies in Geology, 61, pp. 1–18.

Carey, S., 1997. Influence of convective sedimentation on the formation of widespread tephra fall layers in the deep sea. Geology 25, 839–842.

Carey, S., 2000. Volcaniclastic sedimentation around island arcs. In: Sigurdsson, H., Houghton, B., McNutt, S., Rymer, H., Stix, J. (Eds.), Encyclopedia of Volcanoes. Academic Press, New York, pp. 627–642.

Carey, S., Maria, A., Sigurdsson, H., 2000. Use of fractals analysis for discrimination of particles from primary and reworked jökulhlaup deposits in SE Iceland. Journal of Volcanology and Geothermal Research 104, 65–80.

Casadío, S., Feldmann, R., Foland, K., 2000. $^{40}Ar/^{39}Ar$ age and oxygen isotope temperature of the Centinela Formation, southwestern Argentina: An Eocene age for crustacean-rich "Patagonian" beds. Journal of South American Earth Sciences 13, 123–132.

Casadío, S., Griffin, M., Marenssi, S., Net, L., Parras, A., Rodriguez Raising, M., Santillana, S., 2009. Paleontology and sedimentology of middle Eocene rocks in Lago Argentino area, Santa Cruz Province, Argentina. Ameghiniana 46, 27–48.

Crawford, R.S., Casadío, S., Feldmann, R.M., Griffin, M., Parras, A., Schweitzer, C.E., 2008. Mass mortality of fossil decapods within the Monte León Formation (Early Miocene), southern Argentina: victims of Andean volcanism. Annals of Carnegie Museum 77, 259–287.

Cuitiño, J.I., 2011. Registro sedimentológico e isotópico de paleoambientes marinos y transicionales en el Patagoniano (Mioceno) del Lago Argentino. Unpublished PhD Thesis. Buenos Aires University, Argentina, 229 pp.

Cuitiño, J.I., Scasso, R.A., 2010. Sedimentología y paleoambientes del Patagoniano y su transición a la Formación Santa Cruz al sur del Lago Argentino, Patagonia Austral. Revista de la Asociación Geológica Argentina 66, 406–417.

Cuitiño, J.I., Pimentel, M.M., Ventura Santos, R., Scasso, R.A., 2012. High resolution isotopic ages for the "Patagoniense" transgression in southwest Patagonia: stratigraphic implications. Journal of South American Earth Sciences 38, 110–122.

Di Paola, E.C., Marchese, H.G., 1973. Litoestratigrafía de la Formación Patagonia en el área tipo (Bajo de San Julián - Desembocadura del Río Santa Cruz). Provincia de Santa Cruz. República Argentina: 5ª Congreso Geológico Argentino, pp. 207–222 (Actas).

Feruglio, E., 1949. Descripción Geológica de la Patagonia I, II, and III. Dirección General de Yacimientos Petrolíferos Fiscales. T1: 1–323; T2: 1–349; T3: 1–331: Buenos Aires.

Fisher, R.V., Schmincke, H.U., 1984. Pyroclastic Rocks. Springer-Verlag (472 pp.).

Fisher, R.V., Smith, G.A., 1991. Volcanism, tectonics and sedimentation. In: Fisher, R.V., Smith, G.A. (Eds.), Sedimentation in Volcanic Settings. SEPM Special Publication, Tulsa, Oklahoma USA, pp. 1–5.

Fosdick, J.C., Romans, B.W., Fildani, A., Bernhardt, A., Calderón, M., Graham, S.A., 2011. Kinematic evolution of the Patagonian retroarc fold-and-thrust belt and Magallanes foreland basin, Chile and Argentina, 51°30′S. Geological Society of America Bulletin 123, 1679–1698.

Furque, G., 1973. Descripción geológica de la Hoja 58b, Lago Argentino, provincia de Santa Cruz. Boletín, 140. Servicio Nacional Minero Geológico, pp. 1–51.

Furque, G., Camacho, H.H., 1972. El Cretácico Superior y terciario de la región austral del Lago Argentino (Provincia de Santa Cruz). Actas 4º Jornadas Geológicas Argentinas, pp. 61–75.

Gibling, M.R., 2006. Width and thickness of fluvial channel bodies and valley fills in the geological record: a literature compilation and classification. Journal of Sedimentary Research 76, 731–770.

Hayes, S.K., Montgomery, D.R., Newhall, C.G., 2002. Fluvial sediment transport and deposition following the 1991 eruption of Mount Pinatubo. Geomorphology 45, 211–224.

Hervé, F., Pankhurts, R.J., Fanning, C.M., Calderón, M., Yaxley, G.M., 2007. The South Patagonian batholith: 150 my of granite magmatism on a plate margin. Lithos 97, 373–394.

Kataoka, K., 2005. Distal fluvio-lacustrine volcaniclastic resedimentation in response to an explosive silicic eruption: the Pliocene Mushono tephra bed, central Japan. Geological Society of America Bulletin 117, 3–17.

Kataoka, K.S., Manville, V., Nakajo, T., Urabe, A., 2009. Impacts of explosive volcanism on distal alluvial sedimentation: examples from the Pliocene–Holocene volcaniclastic successions of Japan. Sedimentary Geology 22, 306–317.

Kneller, B.C., Branney, M.J., 1995. Sustained high-density turbidity currents and the deposition of thick ungraded sands. Sedimentology 42, 607–616.

Kuenzi, W.D., Horsto, O.H., McGehee, R.V., 1979. Effect of volcanic activity on fluvial–deltaic sedimentation on the modern arc-trench gap, southwestern Guatemala. Geological Society of America Bulletin 90, 827–836.

Le Bas, M.J., Le Maitre, R.W., Woolley, A.R., 1992. The construction of the total alkali-silica chemical classification of volcanic rocks. Mineralogy and Petrology 46, 1–22.

Lirer, L., Vinci, A., 1991. Grain-size distributions of pyroclastic deposits. Sedimentology 38, 1075–1083.

Macellari, C.E., Barrio, C.A., Manassero, M.J., 1989. Upper Cretaceous to Paleocene depositional sequences and sandstone petrography of southwestern Patagonia (Argentina and Chile). Journal of South American Earth Sciences 2, 223–239.

Major, J.J., Janda, R.J., Daag, A.S., 1996. Watershed disturbance and lahars on the east side of Mount Pinatubo during the mid-June 1991 eruptions. In: Newhall, C.G., Punongbayan, R.S. (Eds.), Fire and Mud, Eruptions and Lahars of Mount Pinatubo, Philippines. PHIVOLCS Press, Quezon City, and University of Washington Press, Seattle, pp. 895–920.

Malumián, N., Ardolino, A.A., Franchi, M., Remesal, M., Salani, F., 1999. La sedimentación y el volcanismo terciarios en la Patagonia Extraandina. In: Caminos, R. (Ed.), Geología Argentina. Instituto de Geología y Recursos Minerales: Anales, 29, pp. 557–612.

Manville, V., Newton, E.H., White, J.D.L., 2005. Fluvial responses to volcanism: resedimentation of the 1800a Taupo ignimbrite eruption in the Rangitaiki River catchment, North Island, New Zealand. Geomorphology 65, 49–70.

Manville, V., Németh, K., Kano, K., 2009. Source to sink: a review of three decades of progress in the understanding of volcaniclastic processes, deposits, and hazards. Sedimentary Geology 220, 136–161.

Marenssi, S., Guler, V., Casadío, S., Guerstein, R., Papú, O., 2004. Sedimentology and palynology of the Calafate Formation (Maastrichtian), Austral Basin, Southern Patagonia, Argentina. Cretaceous Research 25, 907–918.

Marenssi, S.A., Limarino, C.O., Tripaldi, A., Net, L.I., 2005. Fluvial systems variations in the Río Leona Formation: tectonic and eustatic controls on the Oligocene evolution of the Austral (Magallanes) Basin, southernmost Argentina. Journal of South American Earth Sciences 19, 359–372.

McPhie, J., Doyle, M., Allen, R., 1993. Volcanic textures: a guide to the interpretation of textures in volcanic rocks. Hobart, CODES Key Centre.University of Tasmania (196 p.).

Miall, A.D., 1996. The geology of fluvial deposits. Sedimentary Facies, Basin Analysis, and Petroleum Geology.Springer-Verlag, Berlin (582 p.).

Mulder, P.J., Alexander, J., 2001. The physical character of subaqueous sedimentary density flows and their deposits. Sedimentology 48, 269–299.

Mulder, T., Syvitski, J.P.M., 1995. Turbidity currents generated at river mouths during exceptional discharges to the world ocean. Journal of Geology 103, 285–299.

Mulder, P.J., Syvitski, J.P.M., Migeon, S., Faugères, S., Savoye, B., 2003. Marine hyperpycnal flows: initiation, behavior and related deposits. A review. Marine and Petroleum Geology 20, 861–882.

Fire and Mud — Eruptions and Lahars of Mount Pinatubo, Philippines. In: Newhall, C.G., Punongbayan, R.S. (Eds.), Philippines Institute of Volcanology and Seismology and the University of Washington Press, Quezon City/Seattle (1126 p.).

Orton, G.J., 1996. Volcanic environments. In: Reading, H.G. (Ed.), Sedimentary Environments: Processes, Facies and Stratigraphy. Blackwell Science, Oxford, pp. 485–567.

Plink-Björklund, P., Steel, R.J., 2004. Initiation of turbidity currents: outcrop evidence for Eocene hyperpycnal flow turbidites. Sedimentary Geology 165, 29–52.

Riggi, J.C., 1978. La importancia de los sedimentos piroclásticos y de la sílice biogenética en la estratigrafía de la Formación Patagonia. Revista de la Asociación Geológica Argentina 33, 158–171.

Sigurdsson, H., Sparks, R.S.J., Carey, S.N., Huang, T.C., 1980. Volcanogenic sedimentation in the Lesser Antilles Arc. Journal of Geology 88, 523–540.

Smith, G.A., 1988. Sedimentology of proximal to distal volcaniclastics dispersed across an active foldbelt: Ellensburg Formation (late Miocene), central Washington. Sedimentology 35, 953–977.

Smith, G.A., 1991. Facies sequences and geometries in continental volcaniclastic sediments. In: Fisher, R.V., Smith, G.A. (Eds.), Sedimentation in Volcanic Settings: SEPM Special Publication, 45, pp. 109–123.

Sumner, E.J., Amy, L.A., Talling, P.J., 2008. Deposit structure and processes of sand deposition from decelerating sediments suspensions. Journal of Sedimentary Research 78, 529–547.

Tanner, W.F., 1967. Ripple mark indexes and their uses. Sedimentology 9, 89–104.

Wetzel, A., 2009. The preservation potential of ash layers in the deep-sea: the example of the 1991-Pinatubo ash in the South China Sea. Sedimentology 56, 1992–2009.

White, J.D.L., Houghton, B.F., 2006. Primary volcaniclastic rocks. Geology 34, 677–680.

Wiesner, M.G., Wang, Y., Zheng, L., 1995. Fallout of volcanic ash to the deep South China Sea induced by the 1991 eruption of Mount Pinatubo (Philippines). Geology 23, 885–888.

Wiesner, M.G., Wetzel, A., Catane, S.G., Listanco, E.L., Mirabueno, H.T., 2004. Grain size, areal thickness distribution and controls on sedimentation of the 1991 Mount Pinatubo tephra layers in the South China Sea. Bulletin of Volcanology 66, 226–242.

Wright, J.V., Mutti, E., 1981. The Dali Ash, Island of Rhodes, Greece: a problem in interpreting submarine volcanogenic sediments. Bulletin of Volcanology 44, 153–168.

Zavala, C., Arcuri, M., Di Meglio, M., Gamero, H., Contreras, C., 2010. A genetic facies tract for the analysis of sustained hyperpycnal flow deposits. In: Slatt, R.M., Zavala, C. (Eds.), Sediment Transfer from Shelf to Deep Water — Revisiting the Delivery SystemAAPG Studies in Geology 61, 31–51.

Zavala, C., Arcuri, M., Blanco Valiente, L., 2012. The importance of plant remains as diagnostic criteria for the recognition of ancient hyperpycnites: Revue de Paléobiologie (Genève), Special, 11, pp. 457–469.

Zernack, A.V., Cronin, S.J., Neall, V.E., Procter, J.N., 2011. A medial to distal volcaniclastic record of an andesite stratovolcano: detailed stratigraphy of the ring-plain succession of south-west Taranaki, New Zealand. International Journal of Earth Sciences 100, 1937–1966.